Rock and Soil Mechanics

Volume 43 | Issue 7 Article 1

9-20-2022

Energy evolution and failure characteristics of single fissure carbonaceous shale under drying–wetting cycles

Xin-xi LIU
School of Civil Engineering, Changsha University of Science and Technology, Changsha, Hunan 410114, China

Yu LI
School of Civil Engineering, Changsha University of Science and Technology, Changsha, Hunan 410114, China, 1986740197@qq.com

Zi-jian FAN
School of Civil Engineering, Changsha University of Science and Technology, Changsha, Hunan 410114, China

Sheng-nan LI
School of Architectural Engineering, Hunan Institute of Engineering, Xiangtan, Hunan 411101, China

See next page for additional authors

Custom Citation

LIU Xin-xi, LI Yu, FAN Zi-jian, LI Sheng-nan, WANG Wei-wei, DONG Peng, . Energy evolution and failure characteristics of single fissure carbonaceous shale under drying–wetting cycles[J]. Rock and Soil Mechanics, 2022, 43(7): 1761-1771.

Energy evolution and failure characteristics of single fissure carbonaceous shale under drying–wetting cycles

Authors

Xin-xi LIU, Yu LI, Zi-jian FAN, Sheng-nan LI, Wei-wei WANG, and Peng DONG

Rock and Soil Mechanics 2022 43(7): 1761−1771 ISSN 1000−7598
https: //doi.org/10.16285/j.rsm.2021.6657 rocksoilmech.researchcommons.org/journal

Energy evolution and failure characteristics of single fissure carbonaceous shale under drying−wetting cycles

LIU Xin-xi[1], LI Yu[1], FAN Zi-jian[1], LI Sheng-nan[2], WANG Wei-wei[1], DONG Peng[1]

1. School of Civil Engineering, Changsha University of Science and Technology, Changsha, Hunan 410114, China
2. School of Architectural Engineering, Hunan Institute of Engineering, Xiangtan, Hunan 411101, China

Abstract: In order to investigate the energy evolution and failure characteristics of carbonaceous shale containing single fissure under drying−wetting cycles, the intact carbonaceous shale samples and the carbonaceous shale samples with fissure angles of 30°, 45° and 60° were prepared. MTS815 rock mechanics test system was used to conduct triaxial compression tests under different drying−wetting cycles. The influence of drying−wetting cycles on the strength, failure mode and energy evolution of single fissure carbonaceous shale were studied. The results show that the elastic energy and dissipated energy at crack initiation stress, damage stress and peak stress present exponential relationships with drying-wetting cycles. The elastic energy and dissipated energy at crack initiation stress and dissipated energy at damage stress are less sensitive to drying−wetting cycle, while the sensitivities of elastic energy at damage stress, and elastic energy and dissipated energy at peak stress are relatively high. The failure mode of carbonaceous shale is dominated by drying−wetting cycle and fissure angle, in which the drying-wetting cycle is the main controlling factor, and the fissure angle is the secondary controlling factor. It is found that tensile shear failure occurs in dry rock sample with fissure angle of 30°, while the dry rock sample with fissure angle of 45°and 60° are subjected to shear failure. With the increase of the number of drying−wetting cycles, the macroscopic length of the main crack increases, the density of secondary cracks increases, and the failure mode transforms to shear-tension composite failure. With the increase of the number of drying−wetting cycles, the energy storage level at crack initiation stress K_{ci} and the energy storage level at damage stress K_{cd} increase gradually. The higher the energy storage level at crack initiation and damage stress, the more likely the crack initiation and rock damage occur. K_{cd} can be used as a warning indicator of rock failure. A larger K_{cd} indicates that the rock is more vulnerable to failure.

Keywords: triaxial compression; single fissure carbonaceous shale; drying−wetting cycle; energy evolution; failure characteristics

1 Introduction

As an important component of highway cutting slope, carbonaceous shale is extensively distributed in the central and southwestern China. Due to seasonal rainfall and evaporation, carbonaceous shale is frequently reshaped by drying−wetting cycles. This process accelerates the strength weakening and structural damage of carbonaceous shale, which poses risks to engineering safety and causes economic losses[1−2]. Therefore, it is of great theoretical significance to understand the mechanical properties and failure mechanism of carbonaceous shale under drying−wetting cycles.

At present, numerous scholars have carried out fruitful research on rock failure and degradation induced by drying−wetting cycles. For example, Liu et al.[3−4] and Fu et al.[5] analyzed the deterioration law of sandstone strength parameters caused by drying−wetting cycles, and investigated the mesoscopic damage by scanning electron microscopy (SEM) and computed tomography (CT) techniques. They found that the uniaxial compressive strength, tensile strength, shear strength, elastic modulus, cohesion and internal friction angle show different deterioration degrees. Song et al.[6] and Xie et al.[7] studied the influence of drying−wetting cycles on sandstone damage characteristics using nuclear magnetic resonance (NMR) method. Song et al.[8] studied the strength weakening law and failure mechanism of weakly consolidated sandstone under drying−wetting cycles using acoustic emission (AE) technology. With the aid of microscope, Yao et al.[9] investigated the sandstone crack propagation under drying−wetting cycles. To sum up, in view of the influence of drying−wetting cycles on rock damage, current research mainly adopts mechanical indices such as strength, elastic modulus, cohesion and internal friction angle, and the approaches mainly rely on NMR, AE, SEM and other technical means. In essence, crack propagation and rock failure under loading involve energy release

Received: 28 September 2021 Revised: 28 March 2022
This work was supported by the National Natural Science Foundation of China (51674041, 52108405) and the Research and Innovation Program for Postgraduates in Hunan Province (SJCX202025).
First author: LIU Xin-xi, male, born in 1963, PhD, professor, PhD supervisor, mainly engaged in the teaching and research of rock and soil stability. E-mail: liuxinxi1963@126.com
Corresponding author: LI Yu, male, born in 1990, PhD candidate, mainly engaged in geotechnical stability evaluation and control. E-mail: 1986740197@qq.com

and dissipation. Therefore, from the perspective of energy, one can better characterize the nature of rock deformation and failure[10−11]. Chen et al.[12], Jiang et al.[13] and Li et al.[14] explored the influence of moisture content on rock energy characteristics, and found that the ultimate energy storage level decreases gradually with the increase of moisture content, and the brittle failure characteristics of rock weakens. Through Brazilian splitting test, Zhang et al.[15] sorted out the influences of moisture content, bedding and pore size on tensile strength and energy of phyllite. Wang et al.[16] carried out uniaxial and triaxial loading and unloading tests on sandstone under different drying−wetting cycles, and stated that with the increase in number of drying−wetting cycles, the total strain energy decreases logarithmically, and the energy difference between dissipated energy and hysteretic cycle is gradually widening.

It is worth noting that the occurrence of numerous fissures in rock mass exerts an important impact on the initiation, propagation and coalescence of cracks and failure modes[17]. Moreover, the determination of rock characteristic stress is of crucial value to reveal the crack evolution. Previous findings manifest a significant influence of drying−wetting cycles on rock mechanical properties, energy and failure characteristics, but there are few studies focusing on the rock energy evolution and failure characteristics considering the drying−wetting cycles and fissure inclination angle (fissure angle for short) simultaneously, especially at the characteristic stress. To address these problems, in this study, triaxial compression tests on carbonaceous shale containing single fissure under drying−wetting cycles are carried out. The characteristic stress of cracks is determined based on the characteristic curve of dissipated energy rate, and the energy evolution of carbonaceous shale containing single fissure during deformation and failure is expounded. The influences of drying−wetting cycles and fissure angle on energy characteristics at characteristic stress are investigated, and the crack evolution and failure characteristics under drying−wetting cycles are revealed. This study could provide a reference for long-term stability early-warning in geotechnical engineering.

2 Methodology

2.1 Sample preparation

The carbonaceous shale was sampled from the Longtang−Langtang highway slope at the chainage K9+800 in Hunan province, China. The collected carbonaceous shale blocks were processed into standard cylindrical cores with a height of 100 mm and a diameter of 50 mm. By means of electronic scale, vernier caliper and nonmetallic ultrasonic nondestructive detector, the density of standard shale samples is measured to be 2.45−2.57 g/cm^3 and the P-wave velocity is 3 065−3 263 m/s. X-ray diffraction (XRD) results suggest that the main mineral components of carbonaceous shale are quartz, illite and kaolinite. Fissures with different inclination angles of 30°, 45° and 60°, length of 20 mm and width of 1 mm were prefabricated at the center of the sample periphery by a high-pressure water jet cutting machine (Fig. 1). The appearance of the processed shale samples was checked, and then the samples with macroscopic defects visible to the naked eye on the surface were removed, thus minimizing the discreteness of the samples.

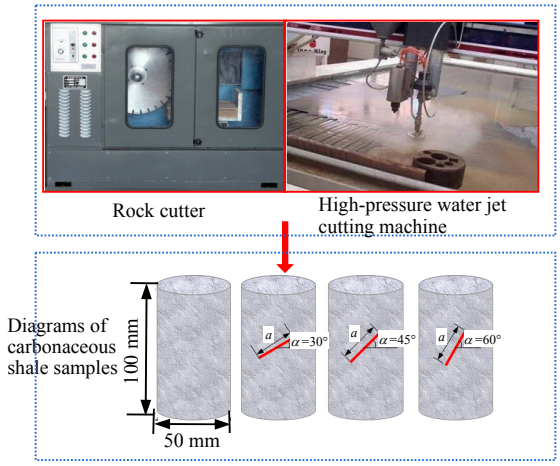

Fig. 1 Carbonaceous shale samples

2.2 Testing scheme

The cyclic drying−wetting tests were conducted following the Chinese standard *Methods for Determining the Physical and Mechanical Properties of Coal and Rock* (GB/T 23561.5−2009)[18]. Firstly, the carbonaceous shale samples were vacuumed for 4 h and absorbed water freely for 20 h. Then, they were placed into an incubator and dried at 60 ℃ for 24 h. The above operation constituted one drying−wetting cycle. In this test, four cyclic tests were carried out with 0, 5, 10 and 15 drying−wetting cycles. The shale samples after cyclic tests were wrapped with plastic film to prevent samples from weathering. Triaxial compression test was performed using MTS815 rock mechanical test system after drying−wetting cycles, as shown in Fig. 2. The samples were divided into four groups according to the number of drying−wetting cycles (0, 5, 10 and 15), each group included an intact shale sample and the samples containing single fissure with fissure angle of 30°, 45° and 60°. Under the confining pressure of 2 MPa, the triaxial compression test was

carried out for each group at a constant loading rate (0.05 MPa/s). After the confining pressure stabilized, the axial stress was applied at a rate of 0.1 kN/s until the sample failed. During the loading, axial and circumferential deformation of shale samples was automatically recorded.

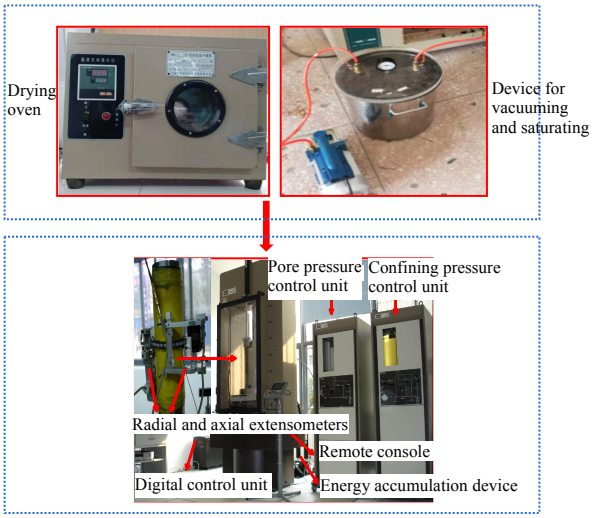

Fig. 2 MTS815 rock mechanics test system

3 Energy evolution of shale after drying−wetting cycles

3.1 Theory of energy calculation

Assuming that the test system is an isolated system without heat exchange with the outside, according to the first law of thermodynamics, the energy absorbed by rock during the test is transformed into elastic energy and dissipated energy[11]:

$$U = U^{\mathrm{e}} + U^{\mathrm{d}} \tag{1}$$

where U is the total energy; U^{e} is the elastic energy; and U^{d} is the dissipated energy.

The relation curve between elastic energy and dissipated energy in the loading process is presented in Fig. 3[12]. The total energy and elastic energy of rock in the principal stress space can be expressed as

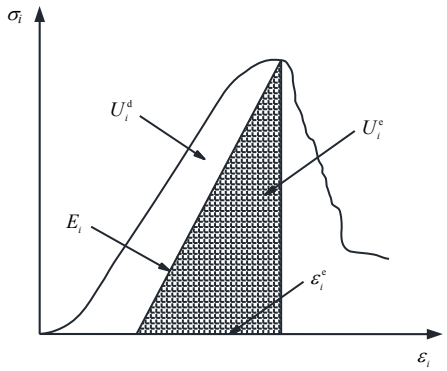

Fig. 3 Relationship between elastic strain energy and dissipated energy of rock mass[12]

$$U = \int_0^{\varepsilon_1} \sigma_1 \mathrm{d}\varepsilon_1 + \int_0^{\varepsilon_2} \sigma_2 \mathrm{d}\varepsilon_2 + \int_0^{\varepsilon_3} \sigma_3 \mathrm{d}\varepsilon_3 \tag{2}$$

$$U^{\mathrm{e}} = \frac{1}{2}\sigma_1\varepsilon_1 + \frac{1}{2}\sigma_2\varepsilon_2 + \frac{1}{2}\sigma_3\varepsilon_3 \tag{3}$$

where σ_1, σ_2 and σ_3 are the first, second and third principal stresses, respectively; and ε_1, ε_2 and ε_3 are the corresponding strains.

According to the Hooke's law, Eq. (3) is transformed into

$$U^{\mathrm{e}} = \frac{1}{2E_{\mathrm{v}}}\left[\sigma_1^2 + \sigma_2^2 + \sigma_3^2 - 2\nu\left(\sigma_1\sigma_2 + \sigma_2\sigma_3 + \sigma_1\sigma_3\right)\right] \tag{4}$$

where E_{v} is the unloading elastic modulus at the linear elastic stage; and ν is the Poisson's ratio. To facilitate calculation, E_{v} is replaced with the initial elastic modulus[19].

Under conventional triaxial compression conditions ($\sigma_2 = \sigma_3$), the total input energy includes the positive work done by σ_1, the positive work U_0 done by hydrostatic pressure and the negative work done by σ_2 and σ_3. By definite integral, the total energy, elastic strain energy and dissipated energy under conventional triaxial compression can be rewritten as

$$U = \int_0^{\varepsilon_1} \sigma_1 \mathrm{d}\varepsilon_1 + 2\int_0^{\varepsilon_3} \sigma_3 \mathrm{d}\varepsilon_3 + U_0 \tag{5}$$

$$U^{\mathrm{e}} = \frac{1}{2E_{\mathrm{v}}}\left[\sigma_1^2 + 2\sigma_3^2 - 2\nu\left(2\sigma_1\sigma_3 + {\sigma_3}^2\right)\right] \tag{6}$$

$$U^{\mathrm{d}} = U - U^{\mathrm{e}} \tag{7}$$

$$U_0 = \frac{3(1-2\nu)}{2E_{\mathrm{v}}}{\sigma_3}^2 \tag{8}$$

3.2 Strength weakening of carbonaceous shale containing single fissure

Given the fact that the stress−strain curves of carboniferous shale with the same fissure angle but different drying−wetting cycles are consistent with those with the same drying−wetting cycles but different fissure angles, the stress−strain curves of fissured shale with 45° fissure angle under different drying−wetting cycles are selected for further analysis, as shown in Fig. 4(a). Figure 4(b) depicts the stress−strain curves of intact and fissured samples after 15 drying−wetting cycles. The stress−strain curves of all samples have experienced initial crack compaction stage (I), linear elastic deformation stage (II), crack stable propagation stage (III), crack accelerated propagation stage (IV) and post-peak failure stage (V). With the increase of the number of drying−wetting cycles, the slope of the curve corresponding to stage II decreases gradually, indicating a decayed

elastic modulus. For dry samples, the post-peak stress drops rapidly at stage V, while the peak stress drop rate decreases and the plastic deformation is enhanced subjected to drying−wetting cycles. Compared with the intact rock sample, the stress−strain curves of fissured samples all move downward, among which the rock sample with 45° fissure angle has the largest drop. According to the variation of peak stress of intact and fissured samples with the number of drying−wetting cycles shown in Fig. 4(c), the drying−wetting cycles and fissure angle have a significant impact on the peak stress of rock samples. With the increase of the number of drying−wetting cycles, the peak stress decreases and the decreasing rate gradually slows down. Under the same drying−wetting cycles (n =15), the peak stresses of rock samples with 30°, 45° and 60° fissure angles decrease by 11.82%, 20.5% and 6.5%, respectively, compared with the peak stress of intact sample (28.76 MPa), suggesting that the prefabricated fissure weakens rock strength, and it decreases first and then rebounds with the increase of fissure angle.

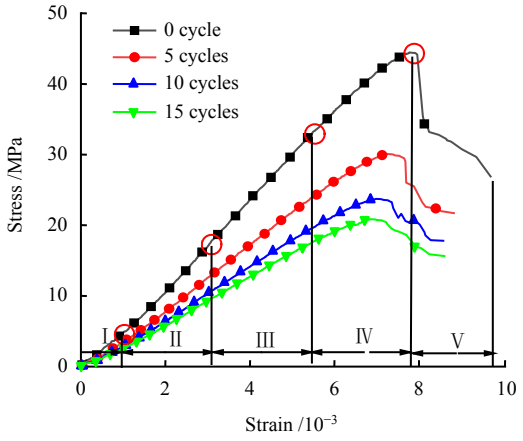

(a) Stress−strain curves of fissured rock samples under different drying−wetting cycles

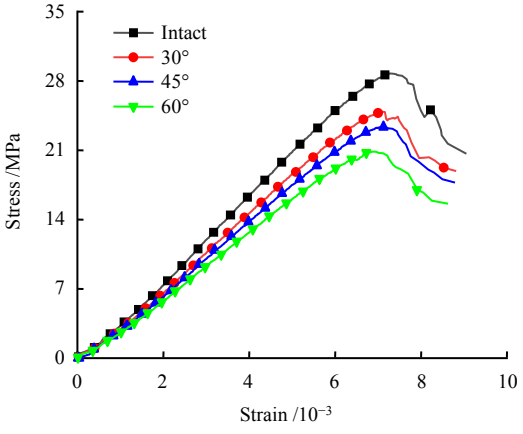

(b) Stress−strain curves of intact and fissured rock samples

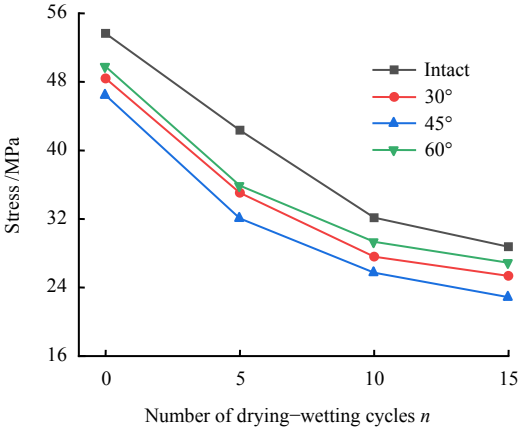

(c) Peak stresses of intact and fissured rock samples

Fig. 4 Triaxial compression test results of intact and fissured rock samples under different drying−wetting cycles

3.3 Energy conversion analysis

In order to quantitatively characterize the conversion between elastic energy and dissipated energy in rock failure process, elastic energy rate U^{e}/U and dissipated energy rate U^{d}/U are defined. In the case of fissure angle of 45°, the relation curves of elastic energy rate and dissipated energy rate with loading stress level under different drying−wetting cycles are plotted in Fig. 5. Under different drying−wetting cycles, the elastic energy rate successively experiences nonlinear decrease, approximately linear increase, nonlinear increase, nonlinear decrease, and sharp decrease, presenting an S-shaped change features, while the dissipated energy rate follows a rigorously opposite trend. Accordingly, the change rule of elastic energy rate and dissipated energy rate during loading can be divided into following five stages.

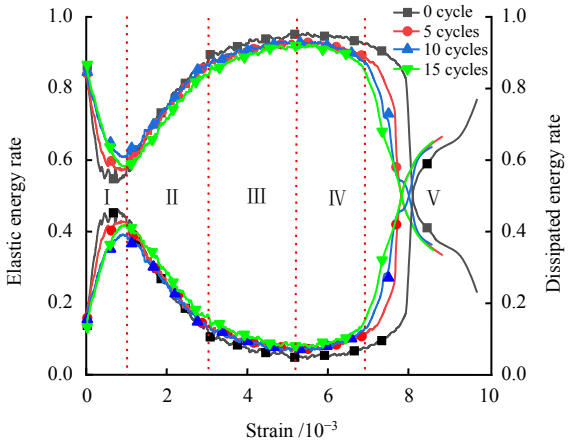

Fig. 5 Variations of elastic energy rate and dissipated energy rate under different drying−wetting cycles

(1) Initial crack compaction stage (I). With increasing strain, the dissipated energy rate increases nonlinearly while the elastic energy rate decreases nonlinearly. This is because the compaction of microcracks and energy dissipation caused by compressive friction between particles, leading to the gradual growth of dissipated energy rate.

(2) Linear elastic deformation stage (II). After the compaction of microcracks, the dissipated energy rate decreases approximately linearly while the elastic energy rate increases approximately, and their difference increases gradually. The reason is that the energy absorbed from the outside is mainly stored in the rock in the form of elastic energy, and the energy dissipated during the initiation and propagation of cracks accounts for a small proportion.

(3) Crack stable propagation stage (III). As the increase in stress level, both the decreasing rate of dissipated energy rate and the increasing rate of elastic energy rate decline, indicating that the increasing rate of elastic energy decreases, while that of dissipated energy increases. Energy tends to dissipate through microcracks propagation, and the rock damage aggravates steadily.

(4) Crack accelerated propagation stage (IV). Plastic deformation dominates rock failure, the internal micro-cracks continue to expand with ever-increasing quantity of cracks and dissipated energy. At this stage, the dissipated energy rate ascends nonlinearly, while the elastic energy rate descends nonlinearly.

(5) Post-peak failure stage (V). After reaching the peak stress, rock failure occurs, along with a significant increase in dissipated energy rate and a sudden drop in elastic energy rate. The difference between the dissipated energy rate and elastic energy rate increases gradually. The elastic energy accumulated in the rock is released instantly, and a sharp increase in the dissipated energy is encountered during the coalescence of cracks and formation of macrocracks.

As displayed in Fig. 6, with the increase of the number of drying−wetting cycles, the growth rate of total absorbed energy decreases with the axial strain, because the more the drying−wetting cycles is, the less the stress required to achieve the same axial strain, the smaller the elastic modulus generated, as well as the lower the growth rate of total absorbed energy is. The more the drying−wetting cycles are, the smaller the total absorbed energy is, the weaker the energy absorption capacity of rock samples is, indicating a limited energy requirement for crack initiation and propagation, and the rock strength also attenuates. Figure 7 shows the evolution curves of total absorbed energy of rock samples with different fissure angles subjected to 15 drying−wetting cycles. The growth rate of total absorbed energy of intact sample with strain is greater than that of fissured samples. Perhaps due to the existence of prefabricated fissure, the samples will produce some initial damage. Meanwhile, local stress concentration occurs under loading, and local damage may reach the failure strength, leading to the overall failure. In contrast, the intact sample is subjected to uniform stress, and the overall failure occurs only when the whole sample is damaged after reaching the failure strength. Therefore, the energy absorption capacity of the intact sample surpasses the fissured samples.

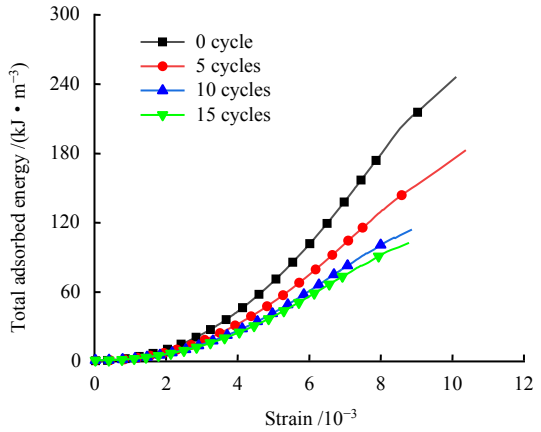

Fig. 6 Evolution curves of total absorption energy under different drying−wetting cycles (α=45°)

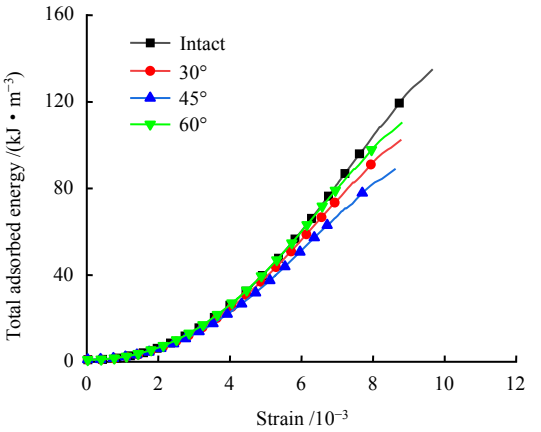

Fig. 7 Evolution curves of total absorption energy under different fissure angles (n=15)

3.4 Determination of characteristic stress

Based on the analysis in Section 3.3, the variation of dissipated energy under different drying−wetting cycles can be divided into five stages, corresponding to the five stages of rock deformation and failure. Next, the sample with fissure angle of 45° and 15 drying−wetting cycles is taken as the example to analyze the relationship between dissipated energy rate and strain (Fig. 8), in order to determine the characteristic stress of carbonaceous shale. There exists a maximum value and a minimum value on the dissipated energy rate-strain curve, which can be regarded as crack closure stress σ_{cc} and damage stress σ_{cd}, respectively. The inflection point of dissipated energy rate−strain curve from linear decrease to nonlinear decrease serves as the crack initiation stress σ_{ci}.

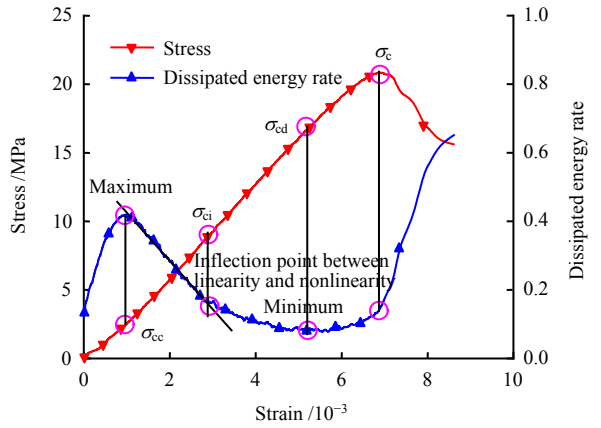

Fig. 8 Determination of characteristic stress using dissipated energy rate (α=45°, n=15)

In order to verify the rationality of the proposed method that determines the characteristic stress using dissipated energy rate characteristic curve, the ratios of crack closure stress, crack initiation stress and damage stress to peak stress under different conditions are compared, as listed in Table 1. The mean values of σ_{cc}/σ_c, σ_{ci}/σ_c and σ_{cd}/σ_c are 16.06%, 44.59% and 77.07%, respectively, and the variances are merely 0.04%, 0.02% and 0.03%, respectively, confirming a minimal data dispersion of the proposed method. Previous results[20−21] show that the crack closure stress, crack initiation stress and damage stress are about 15%−20%, 30%−50% and 70%−80% of the peak stress, respectively. The characteristic stresses determined by the dissipated rate characteristic curve all fall in a reasonable range, verifying its rationality and enriching the methods for determining the characteristic stress.

Table 1 Characteristic stresses of rock samples under different conditions

Fissure angle /(°)	Number of drying−wetting cycles	σ_c / MPa	$\frac{\sigma_{cc}}{\sigma_c}$ /%	$\frac{\sigma_{ci}}{\sigma_c}$ /%	$\frac{\sigma_{cd}}{\sigma_c}$ /%
Intact	0	53.66	15.13	43.31	73.79
	5	42.35	14.92	43.00	76.53
	10	32.14	17.24	45.77	77.13
	15	28.76	18.13	44.71	78.06
30	0	48.39	12.92	42.24	75.60
	5	35.05	14.8%	43.19	76.53
	10	27.60	17.80	45.87	77.11
	15	25.36	18.01	46.34	78.47
45	0	46.44	12.15	41.56	75.18
	5	32.07	16.10	45.93	75.68
	10	25.73	18.27	46.17	80.35
	15	22.87	19.13	46.53	80.97
60	0	49.79	13.52	43.58	75.57
	5	35.68	14.84	44.28	75.99
	10	29.32	16.83	45.26	77.78
	15	26.89	17.17	45.78	78.30

3.5 Energy evolution at characteristic stress

According to the proposed method of determining characteristic stress of carbonaceous shale using characteristic curve of dissipated energy rate, the elastic energy and dissipated energy at corresponding characteristic stresses are obtained. The elastic energy and dissipated energy corresponding to crack initiation stress, damage stress and peak stress are denoted as U_{ci}^e, U_{cd}^e, U_c^e and U_{ci}^d, U_{cd}^d, U_c^d, respectively. Figures 9 and 10 display the relationship of elastic energy and dissipated energy at each characteristic stress with the number of drying−wetting cycles.

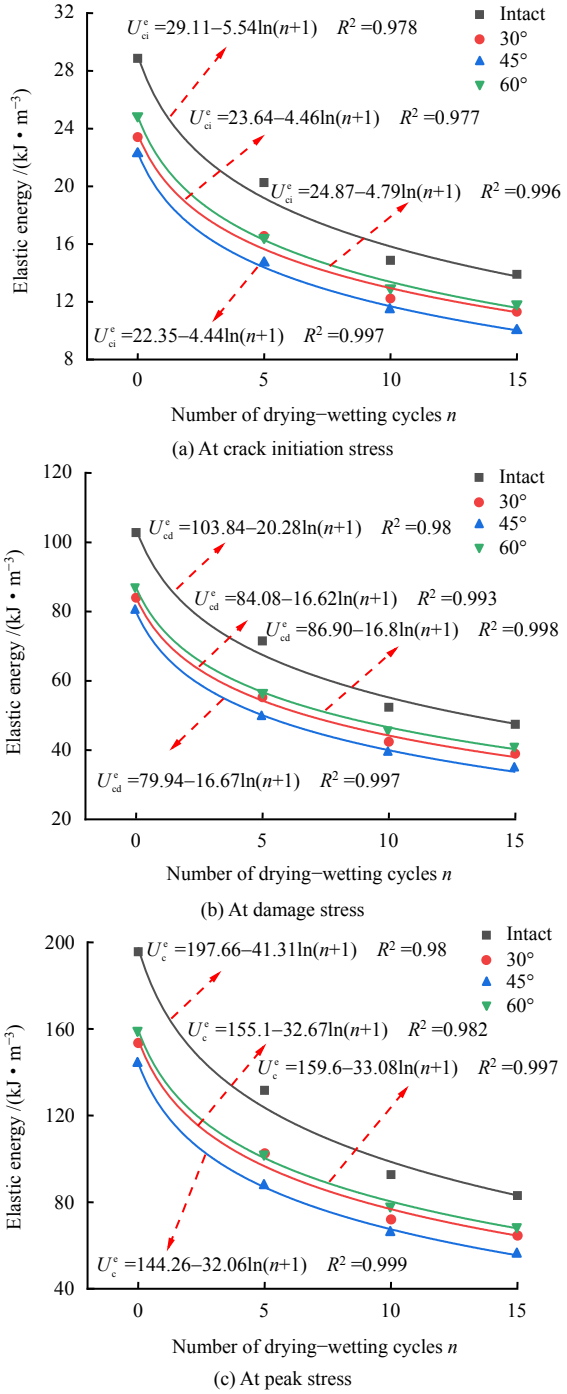

Fig. 9 Variation curves of elastic energy corresponding to each characteristic stress point with n

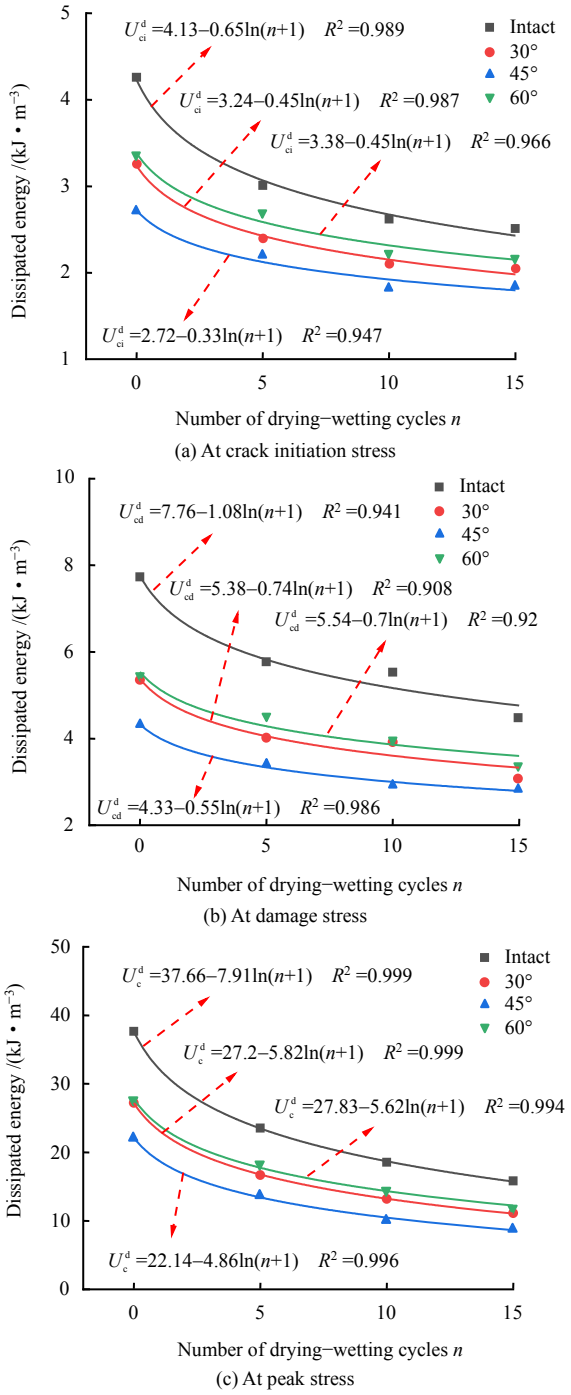

Fig. 10 Variation curves of dissipated energy corresponding to each characteristic stress point with *n*

In Figs. 9 and 10, the elastic energy and dissipated energy at each characteristic stress decrease at a decreasing rate with the increase in number of drying−wetting cycles. In detail, at each characteristic stress, the elastic energy and dissipated energy of fissured samples are smaller than that of intact one, increasing first and then decreasing with the minimum at 45°. Due to the existence of prefabricated fissure and the increase in number of drying−wetting cycles, less energy is stored and dissipated at the pre-peak deformation stage, indirectly reflecting that the drying−wetting cycles and prefabricated fissure reduce the yield strength of carbonaceous shale. This is because the damage of the carbonaceous shale is aggravated and its internal structure becomes looser due to repeated drying and wetting. Prefabricated fissure causes irreversible damage to shale samples as well as stress concentration, leading to overall failure eventually. As a result, less energy needs to be stored and dissipated during crack propagation and coalescence until macroscopic failure. Through the least squares method, it is found that the elastic energy and dissipated energy at each characteristic stress follow an exponential function with the number of drying−wetting cycles. The goodness of fit is above 0.90 in all cases. The fitting function is written as

$$Y = a - b\ln(n+1) \tag{9}$$

where Y is the elastic energy and dissipated energy at the characteristic stress; and a and b are the fitting coefficients.

According to Eq. (9), the sensitivities of elastic energy and dissipated energy at each characteristic stress to the number of drying−wetting cycles are related to the fitting coefficient b, and in general, the sensitivity is positively correlated with b. According to the fitting results in Figs. 9 and 10, the values of fitting coefficient b of intact and fissured samples are obtained, as shown in Fig. 11. The sensitivity of elastic energy at crack initiation stress U_{ci}^{e} to the number of drying−wetting cycles is low, while those at damage stress U_{cd}^{e} and peak stress U_{c}^{e} are relatively high. In Fig. 11(b), the dissipated energy values at crack initiation stress U_{ci}^{d} and damage stress U_{cd}^{d} are less sensitive to the number of drying−wetting cycles, while that at peak stress U_{c}^{d} is more sensitive. Cracks have a significant impact on the fitting coefficient b at the peak stress; in contrast, it barely affects b at the crack initiation stress and damage stress. Moreover, the sensitivity of U_{c}^{d} to fissure angle at peak stress is higher than that of U_{c}^{e}.

In the triaxial compression test, the ratios of elastic energy at crack initiation stress and damage stress to that at peak stress reflect the energy storage status at different stages, which are defined as the energy storage level at crack initiation stress K_{ci} ($K_{ci} = U_{ci}^{e}/U_{c}^{e}$) and damage stress K_{cd} ($K_{ci} = U_{cd}^{e}/U_{c}^{e}$). Figure 12 presents the curves of K_{ci} and K_{cd} in relation to the number of drying−wetting cycles n. With the increase of n, K_{ci} and K_{cd} gradually increase, indicating that the higher the energy storage level at the crack initiation stress and damage stress, the easier the crack initiation and damage. Compared with the intact sample, the buildup of K_{ci} and K_{cd} for fissured samples is more obvious, reaching the peak when the fissure angle is 45°. The results reveal

that the crack initiation stress and damage stress are closely linked to the energy storage capacity at the characteristic stress, which is affected by the number of drying−wetting cycles and fissure angle directly. K_{cd} represents the relative range of energy storage from unstable crack propagation to overall failure, and can be used as a warning indicator of rock failure. The buildup of K_{cd} indicates that the stored energy of rock sample is close to the ultimate energy storage, and the damage is more likely to occur.

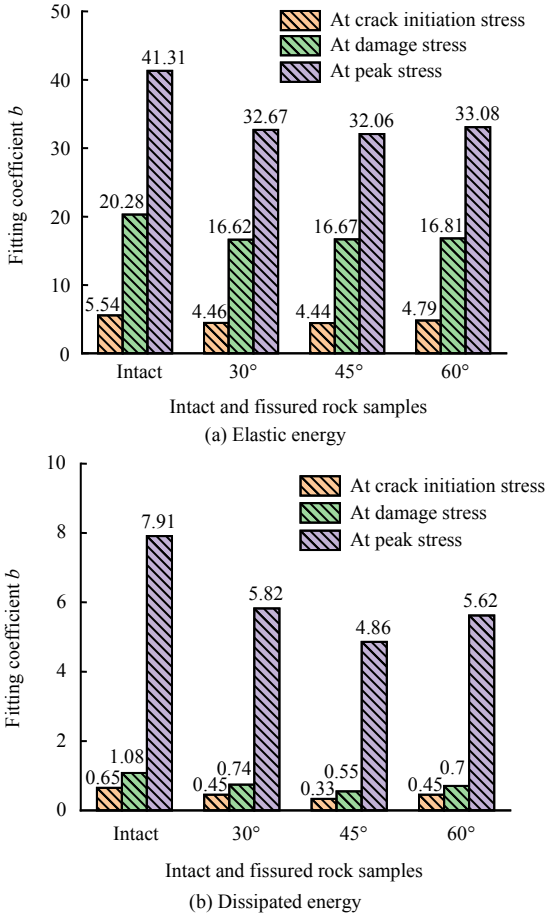

Fig. 11 Relationships between fitting coefficient *b* and fissure angle *α*

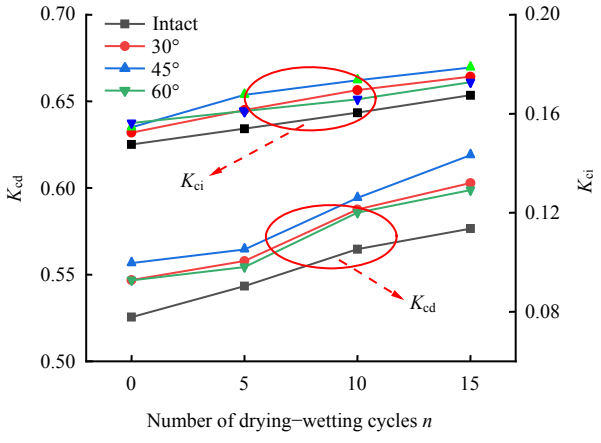

Fig. 12 Variation curves of K_{ci} and K_{cd} with *n*

4 Failure mechanism of fissured shale after drying−wetting cycles

4.1 Crack evolution and failure mode

Figure 13 illustrates the macroscopic crack development of intact and fissured carboniferous shale subjected to drying−wetting cycles. The main cracks are marked in red, and the secondary cracks are marked in green. After multiple drying−wetting cycles, tensile cracks appear at the top and shear cracks cut throughout the top and bottom of the intact samples (Fig. 13(a)). The cracks formed in fissured samples are more complicated than those in intact sample. Taking the sample with the fissure angle of 30° after 15 drying−wetting cycles as an example, the crack types are composed of wing crack ①, non-coplanar secondary crack ④ and far-field crack ⑥, and the failure mode is tensile−shear type (Fig. 13(b)). The general characteristics of the crack evolution are that the wing cracks produced by tension appear first, but it is not the cause of the final failure of shale samples. Taking the sample with fissure angle of 45° as an example, after 10 drying−wetting cycles, the wing crack ① and anti-tensile crack ② will develop into coplanar secondary crack ③ and non-coplanar secondary crack ④ due to stress concentration, resulting in tensile−shear failure (Fig. 13(c)). As a special tensile crack, crack ② is often accompanied by crack ①, such as samples with fissure angles of 30° and 45° after 10 drying−wetting cycles. Non-coplanar secondary crack ④ is the main type of crack encountered in shear failure, and the frequency of crack ④ in all fissured samples increases with the increase in number of drying−wetting cycles. However, for the dry sample, when the fissure angle increases from 30° to 60°, crack ④ turns to crack ③, and the crack initiation angle (the included angle between the macrocrack and the prefabricated fissure) gradually tapers. In addition, transverse crack ⑤ appears in the sample with 45° fissure angle after 0 and 5 drying−wetting cycles; however, it does not reach the boundary, but is transformed into crack ④ (Fig. 13(c)).

It is necessary to analyze the ultimate failure modes of fissured carbonaceous shale in addition to the types of cracks. According to the triaxial compression test results, the final failure modes of intact and fissured shale samples under different drying−wetting cycles mainly include shear failure, tensile−shear failure and shear−tensile failure. When the fissure angle increases from 30° to 60°, the failure of dry sample develops from tensile−shear failure to shear failure. With the increase in number of drying−wetting cycles, the macroscopic length of the main cracks increases, the secondary cracks become dense, and the failure mode

develops to shear−tensile failure. This illustrates that the drying−wetting cycles has more control over the crack evolution and failure mode than the fissure angle. The number of drying−wetting cycles is the primary controlling factors while the fissure angle is secondary. The reason is that under repeated drying−wetting cycles, the dissolution of clay minerals in carbonaceous shale leads to the initiation and propagation of internal microcracks, whilst the well-developed microcracks result in the rise of secondary cracks under confining pressure. Additionally, consecutive drying−wetting cycles aggravate the damage near the prefabricated fissure and put a brake on stress concentration. Crack propagation within rock, as a consequence, is weakened by stress relief, resulting in the weakening of the control effect of fissure angle.

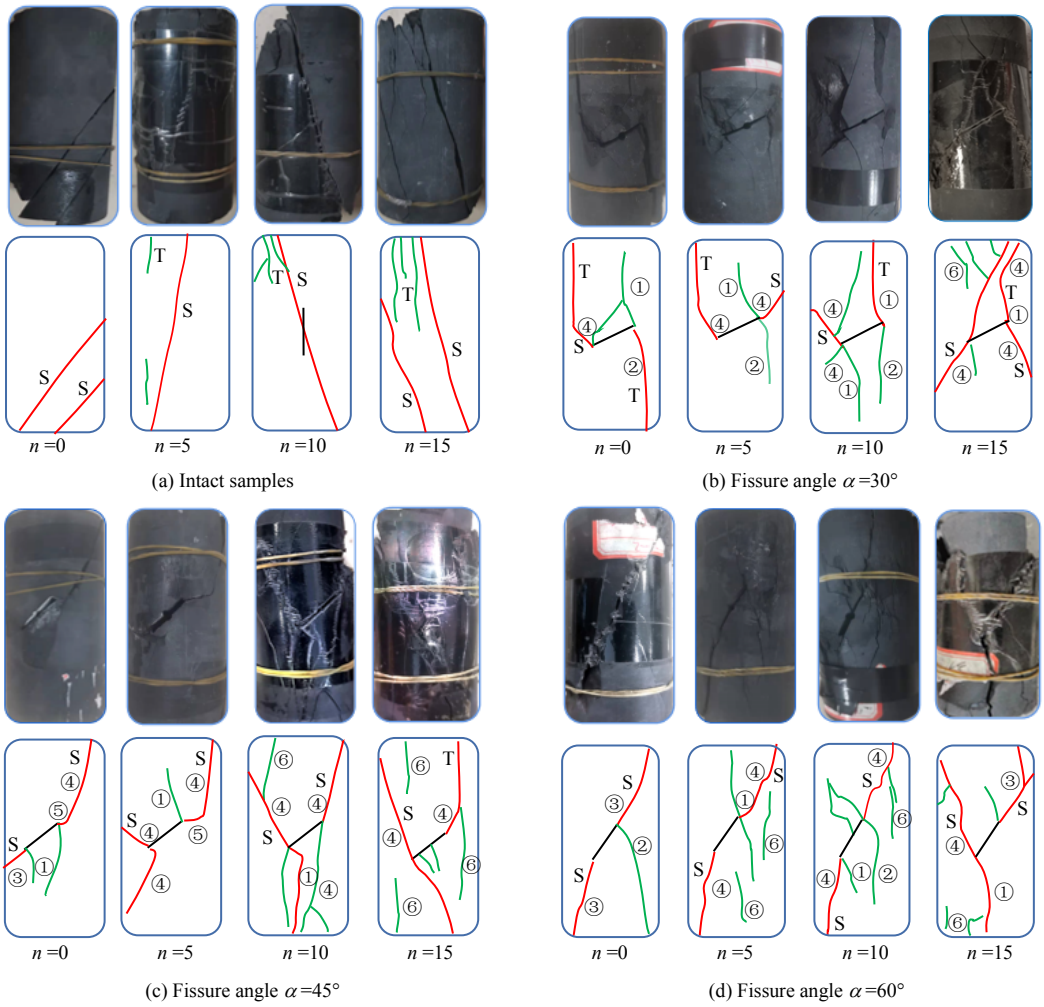

Note: ①: Wing crack, ②: Anti-tensile crack, ③: Coplanar secondary crack, ④: Non-coplanar secondary crack, ⑤: Transverse crack, ⑥: Far-field crack, T: Tensile, S: Shear

Fig. 13 Failure patterns of carbonaceous shale under triaxial compression

4.2 Mechanism of crack initiation

Fissured rock mass mainly presents the compression shear fracture, and the crack propagation belongs to the I+II compression shear composite fracture. It is assumed that the length of the prefabricated fissure is $2a$, the fissure angle is α, affected by the far-field maximum and minimum principal stresses σ_1 and σ_3. According to the definition, stress intensity factors K_{I} and K_{II} are expressed as

$$K_{\mathrm{I}}=(\sigma_1\cos^2\alpha+\sigma_3\sin^2\alpha)\sqrt{\pi a} \tag{10}$$

$$K_{\mathrm{II}}=(\sigma_1-\sigma_3)\sin\alpha\cos\alpha\sqrt{\pi a} \tag{11}$$

According to the maximum circumferential stress criterion[22], the relation of stress intensity factors of I+II composite crack can be obtained through

$$\frac{K_{\mathrm{II}}}{K_{\mathrm{I}}}=\frac{\sin\theta}{1-3\cos\theta} \tag{12}$$

where θ is the crack initiation angle.

In Eqs. (10) and (11), σ_1 is substituted by crack initiation stress σ_{ci}, and based on the test data in Table 1, variation curves of $K_{\mathrm{II}}/K_{\mathrm{I}}$ and fissure angle under different drying−wetting cycles are obtained, as shown in Fig. 14. Taking the derivative of the

right-hand side of Eq. (12), it is found that with the increase of $K_{\mathrm{II}}/K_{\mathrm{I}}$, crack initiation angle decreases gradually, whereas with the increase of fissure angle, $K_{\mathrm{II}}/K_{\mathrm{I}}$ grows steadily (Fig. 14), further indicating that the crack initiation angle decreases with the increase of fissure angle, which is consistent with the test results.

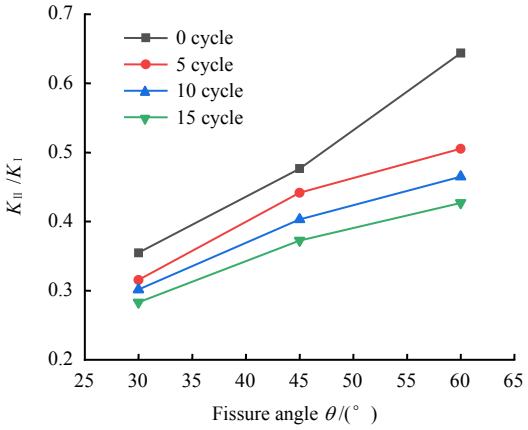

Fig. 14 Variation curves of $K_{\mathrm{II}}/K_{\mathrm{I}}$ with fissure angle

4.3 Energy driving mechanism of rock failure after drying−wetting cycles

According to the energy driving mechanism, rock failure occurs when the accumulated energy inside the rock reaches its ultimate energy storage[10]. Hence, it is imperative to have an insight into the energy storage characteristics of fissured carbonaceous shale under drying−wetting cycles. Figure 15 illustrates the relationship between peak elastic energy and number of drying−wetting cycles and fissure angle. Taking the dry sample with 30° fissure angle for example, the peak elastic energy reaches up to 152.6 kJ/m^3. After 5, 10 and 15 cycles, the decreasing rate is 32.78%, 52.73% and 57.66%, respectively. It suggests that the increase in number of drying−wetting cycles will diminish the ultimate energy storage of shale samples and substantially weaken the resistance capability of deformation and failure. Combining with Fig. 13(b), it is found that with the increase in number of drying−wetting cycles, the cohesion of shale samples decreases and the microstructure damage occurs. Secondary cracks increase along with obvious surface roughening. The energy stored and released in shale samples reduces synchronously, and the ductility failure characteristics are enhanced. With the increase of fissure angle, the ultimate energy storage of shale samples decreases first and then increases, reaching the minimum at 45° fissure angle. Essentially, with the increase of fissure angle, the resistance capability of deformation and failure reduces first, followed by an increase, and the more the number of drying−wetting cycles, the less the impact of fissure angle on the ultimate energy storage. Overall, the macroscopic failure of fissured shale samples with different fissure angles is shear−tensile failure (Fig. 13). It manifests that the failure characteristics of shale samples are closely related to the stored energy, and indirectly embodies the influences of drying−wetting cycles and fissure angle on the stored energy and failure characteristics. This warns us that during the construction and design of tunnel, slope and chamber rock mass engineering, sufficient attention should be paid to the influences of water content and occurrence difference of fractured rock mass to guarantee the safety and stability of the project.

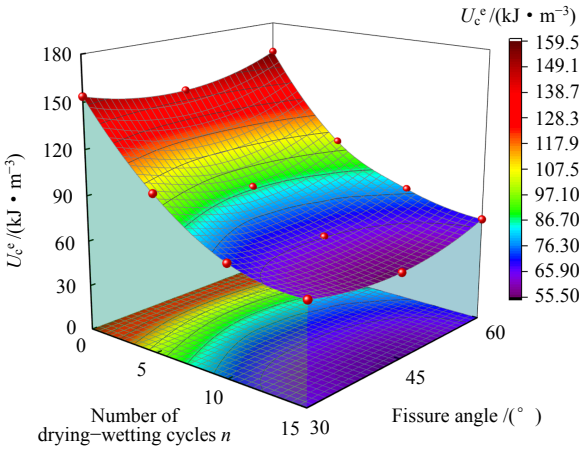

Fig. 15 Variation curves of peak elastic energy with number of drying−wetting cycles and fissure angles

5 Conclusions

(1) Crack closure stress, initiation stress and damage stress were determined based on the characteristic curve of dissipated energy rate, which laid a foundation for the following study on the influence mechanism of drying−wetting cycles and fissure angle on the characteristic stress, and energy response at characteristic stress.

(2) With the increase in number of drying−wetting cycles, the elastic energy and dissipated energy at crack initiation stress, damage stress and peak stress gradually decline at a decreasing rate. $U_{\mathrm{ci}}^{\mathrm{e}}$, $U_{\mathrm{ci}}^{\mathrm{d}}$ and $U_{\mathrm{cd}}^{\mathrm{d}}$ are less sensitive to drying−wetting cycles, whereas $U_{\mathrm{cd}}^{\mathrm{e}}$, $U_{\mathrm{c}}^{\mathrm{e}}$ and $U_{\mathrm{c}}^{\mathrm{d}}$ are more sensitive.

(3) The failure mode of carbonaceous shale is controlled by the number of drying−wetting cycles and fissure angle. The former is the primary controlling factor, while the latter is secondary. When the fissure angle increases from 30° to 60°, the failure of dry shale sample develops from tensile−shear failure to shear failure. With the increase in number of drying−wetting cycles, the macroscopic length of the main crack increases, the number of secondary cracks

increases, and the failure mode shifts to shear−tensile failure.

(4) K_{ci} and K_{cd} continue upward with the increase in number of drying−wetting cycles, indicating that the higher the energy storage level at the crack initiation stress and damage stress, the easier the crack initiation and rock damage. K_{cd} can be used as a warning indicator of rock failure, and the likelihood of rock failure goes up with the increase of K_{cd}.

References

[1] ZHOU Cui-ying, PENG Ze-ying, SHANG Wei, et al. On the key problem of the water-rock interaction in geoengineering: mechanical variability of special weak rocks and some development trends[J]. Rock and Soil Mechanics, 2002, 23(1): 124−128.

[2] ZHOU Hui, FENG Xia-ting. Advances in coupled mechanical-hydro-chemical processes in rocks[J]. Chinese Journal of Rock Mechanics and Engineering, 2006, 25(4): 855−865.

[3] LIU Xin-rong, LI Dong-liang, WANG Zhen, et al. The effect of dry-wet cycles with acidic wetting fluid on strength deterioration of shaly sandstone[J]. Chinese Journal of Rock Mechanics and Engineering, 2016, 35(8): 1543−1554.

[4] LIU Xin-rong, YUAN Wen, FU Yan, et al. Tests on shear strength deterioration of sandstone under the action of chemical solution and drying−wetting cycles and analysis of chemical thermodynamics[J]. Chinese Journal of Rock Mechanics and Engineering, 2016, 35(12): 2534−2541.

[5] FU Yan, WANG Zi-juan, LIU Xin-rong, et al. Meso damage evolution characteristics and macro degradation of sandstone under wetting−drying cycles[J]. Chinese Journal of Geotechnical Engineering, 2017, 39(9): 1653−1661.

[6] SONG Yong-jun, ZHANG Lei-tao, REN Jian-xi, et al. Study on damage characteristics of weak cementation sandstone under drying−wetting cycles based on nuclear magnetic resonance technique[J]. Chinese Journal of Rock Mechanics and Engineering, 2019, 38(4): 825−831.

[7] XIE Kai-nan, JIANG De-yi, SUN Zhong-guang, et al. Influence of drying−wetting cycles on microstructure degradation of shaly sandstone using nuclear magnetic resonance[J]. Rock and Soil Mechanics, 2019, 40(2): 653−659, 667.

[8] SONG Chao-yang, JI Hong-guang, JIANG Hua, et al. Influence of wetting−drying cycles on acoustic emission characteristics and microstructure deterioration of weak cementation stratum[J]. Journal of China Coal Society, 2018, 43(Suppl. 1): 96−103.

[9] YAO Hua-yan, ZHU Da-yong, ZHOU Yu-xin, et al. Real-time observation and analysis of fracturing process of sandstone under cyclic drying and wetting[J]. Rock and Soil Mechanics, 2013, 34(2): 329−336.

[10] XIE He-ping, PENG Rui-dong, JU Yang, et al. On energy analysis of rock failure[J]. Chinese Journal of Rock Mechanics and Engineering, 2005, 24(15): 2603−2608.

[11] LI Xin-wei, YAO Zhi-shu, HUANG Xian-wen, et al. Investigation of deformation and failure characteristics and energy evolution of sandstone under cyclic loading and unloading[J]. Rock and Soil Mechanics, 2021, 42(6): 1693−1704.

[12] CHEN Zi-quan, HE Chuan, WU Di, et al. Mechanical properties and energy damage evolution mechanism of deep-buried carbonaceous phyllite[J]. Rock and Soil Mechanics, 2018, 39(2): 445−456.

[13] JIANG Jing-dong, CHEN Sheng-shui, XU Jie, et al. Mechanical properties and energy characteristics of mudstone under different containing moisture states[J]. Journal of China Coal Society, 2018, 43(8): 2217−2224.

[14] LI Tian-bin, CHEN Zi-quan, CHEN Guo-qing, et al. An experimental study of energy mechanism of sandstone with different moisture contents[J]. Rock and Soil Mechanics, 2015, 36(Suppl. 2): 229−236.

[15] ZHANG Chuang, REN Song, ZHANG Ping, et al. Experimental study on Brazilian splitting of phyllite under coupling effects of water, pore and bedding[J]. Rock and Soil Mechanics, 2021, 42(6): 1612−1624.

[16] WANG Zi-juan. Damage evolution characteristics and the accumulation damage model of sandstone under dry-wet cycle[D]. Chongqing: Chongqing University, 2016.

[17] YANG S Q. Crack coalescence behavior of brittle sandstone samples containing two coplanar fissures in the process of deformation failure[J]. Engineering Fracture Mechanics, 2011, 78(17): 3059−3081.

[18] The National Standard Compilation Groups of People's Republic of China. GB/T 23561.5－2009 Methods for determining the physical and mechanical properties of coal and rock[S]. Beijing: China Quality and Standards Publishing & Media Co., Ltd., 2009.

[19] YOU Ming-qing, SU Cheng-dong. Experimental study on strengthening of marble specimen in cyclic loading of uniaxial or pseudo-triaxial compression[J]. Chinese Journal of Solid Mechanics, 2009, 29(1): 66−72.

[20] LEI X, QIN S, SUN Q, WANG Y Y, et al. A study on crack damage stress thresholds of different rock types based on uniaxial compression tests[J]. Rock Mechanics and Rock Engineering, 2014, 47(4): 1183−1195.

[21] LIU Quan-sheng, HU Yun-hua, LIU Bin. Progressive damage constitutive models of granite based on experimental results[J]. Rock and Soil Mechanics, 2009, 30(2): 289−296.

[22] ERDOGAN F, SIH G C. On the crack extension in plates under plane loading and transverse shear[J]. Journal of Basic Engineering, 1963, 85(4): 519−525.